Journal of Inflammation Research

Dovepress
Taylor & Francis Group

Open Access Full Text Article

ORIGINAL RESEARCH

Identification and Validation of Lipid Metabolism-Related Biomarkers GPD1 and CEBPD in Metabolic Dysfunction-Associated Steatohepatitis

Jianyu Zhou[1,*], Chunying Xiao[1,*], Bin Huang[2], Fenfang Chen[3,4]

[1]Department of Ultrasound, Taizhou Central Hospital (Taizhou University Hospital), School of Medicine, Taizhou, Zhejiang, People's Republic of China; [2]Department of Radiology, Taizhou Central Hospital (Taizhou University Hospital), School of Medicine, Taizhou, Zhejiang, People's Republic of China; [3]Department of Infectious Diseases, Taizhou Hospital of Zhejiang Province Affiliated to Wenzhou Medical University, Taizhou, Zhejiang, People's Republic of China; [4]Department of Infectious Diseases, Enze Hospital, Taizhou Enze Medical Central (Group), Taizhou, Zhejiang, People's Republic of China

*These authors contributed equally to this work

Correspondence: Fenfang Chen, Department of Infectious Diseases, Taizhou Hospital of Zhejiang Province Affiliated to Wenzhou Medical University, Taizhou, Zhejiang, People's Republic of China, Email chenfenf@enzemed.com

Background: Metabolic dysfunction-associated steatohepatitis (MASH) remains a major clinical challenge due to the lack of effective diagnostic biomarkers and therapeutic targets. Identifying and validating key lipid metabolism-related genes may offer novel strategies for the early diagnosis and targeted treatment of MASH.

Methods: In this study, differentially expressed genes (DEGs) were identified from public databases using integrated bioinformatics approaches. Weighted gene co-expression network analysis (WGCNA) and multiple machine learning algorithms were employed to screen for hub genes closely associated with MASH. The expression levels and diagnostic potential of the candidate genes GPD1 and CEBPD were systematically evaluated through nomogram construction, immune infiltration analysis, and both in vivo and in vitro experiments. Their biological functions were further validated at the cellular level.

Results: The results revealed a strong association between lipid metabolism dysregulation and alterations in immune cell composition in MASH. GPD1 was significantly upregulated and CEBPD was downregulated in both the MASH animal and cell models, and both genes showed good diagnostic value. Functional experiments demonstrated that knockdown of GPD1 in HepG2 cells significantly reduced lipid accumulation, inflammatory responses, and expression of fibrosis-related markers. Similarly, overexpression of CEBPD also inhibited these pathological processes, indicating that both GPD1 and CEBPD play critical roles in MASH progression.

Conclusion: This study highlights the importance of GPD1 and CEBPD as potential diagnostic biomarkers and therapeutic targets for MASH, providing a theoretical and experimental foundation for improving early diagnostic strategies and developing interventions targeting inflammation and lipid metabolism dysregulation in metabolic liver disease.

Keywords: metabolic dysfunction-associated steatotic liver disease, metabolic dysfunction-associated steatohepatitis, lipid metabolism, GPD1, CEBPD

Introduction

According to reliable data, approximately 840 million individuals worldwide suffer from chronic liver disease, with about 2 million deaths occurring annually due to this condition.[1] In recent years, Metabolic dysfunction-associated steatotic liver disease (MASLD) has gained increasing attention and is gradually replacing viral infections as the leading cause of chronic liver disease.[2–4] The global prevalence of MASLD is approximately 25%–30%, with rates in Chinese adults reaching 29%–32%.[5–7] Individuals with obesity, type 2 diabetes, and metabolic syndrome are considered high-risk populations. MASLD can

Received: 21 February 2025
Accepted: 4 October 2025
Published: 25 October 2025

progress to metabolic dysfunction-associated steatohepatitis (MASH), which may further lead to liver fibrosis, cirrhosis, and even hepatocellular carcinoma. In addition to liver-related complications, MASLD is closely associated with various extrahepatic conditions, including cardiovascular disease, type 2 diabetes, and chronic kidney disease, making it a significant global public health concern.[8] Notably, the pathogenesis of liver fibrosis and chronic liver disease progression resulting from fatty liver degeneration differs from the mechanisms underlying chronic liver disease induced by viral infections and aflatoxin toxicity.[9–11] MASLD represents a broader spectrum of metabolic dysfunction-associated steatotic liver disease, while MASH is a progressive subtype within MASLD characterized by inflammation and a high risk of fibrosis. Therefore, accurate diagnosis of MASH is crucial for the stratified management of patients with MASLD.

A more pressing concern is the current limitation in diagnostic methods for MASLD, MASH, and liver fibrosis. Conventional imaging techniques, such as ultrasound and CT scans, can only provide a general estimate of the severity and distribution of fatty liver but cannot distinguish between MASLD and MASH.[12] Although liver biopsy remains the gold standard for diagnosing and assessing the severity of liver fat degeneration, its invasiveness necessitates the exploration of non-invasive diagnostic alternatives, and its invasive nature significantly limits its clinical applicability. Therefore, identifying novel biomarkers for MASH and elucidating the molecular mechanisms driving MASLD/MASH progression is essential for advancing diagnostic and therapeutic strategies.[13]

Abnormal lipid metabolism, resulting in excessive fat accumulation, is a defining characteristic of MASLD.[14] In the pathogenesis of MASLD, dysregulated lipid metabolism plays a central role. Insulin resistance enhances lipolysis in adipose tissue, resulting in excessive influx of free fatty acids into the liver.[15] Concurrently, de novo lipogenesis (DNL) is upregulated, fatty acid oxidation is impaired, and the export of very low-density lipoproteins (VLDL) is reduced, collectively leading to abnormal accumulation of triglycerides within hepatocytes. Moreover, mitochondrial dysfunction and oxidative stress exacerbate lipotoxicity, triggering inflammatory responses and hepatocellular injury, thereby promoting the progression of MASLD to MASH and liver fibrosis.[16] Reversing early hepatic steatosis can partially mitigate the progression of MASH and liver fibrosis, highlighting the importance of lipid metabolism regulation in the prevention and treatment of both conditions.[15] GPD1 (Glycerol-3-phosphate dehydrogenase 1) is a key enzyme involved in glycerol metabolism and plays a crucial role in regulating cellular lipid homeostasis and redox balance.[17] Overexpression of GPD1 can enhance triglyceride synthesis, exacerbating hepatic steatosis, a hallmark of early-stage MASH10. Dysregulated GPD1 disrupts lipid storage and distribution, leading to intracellular lipid accumulation, lipotoxicity, inflammation, and hepatocyte damage.[18] Furthermore, excessive GPD1 activity may increase the production of reactive oxygen species (ROS), inducing oxidative stress, damaging hepatocytes, impairing insulin signaling pathways, and exacerbating insulin resistance.[19] CEBPD (CCAAT/enhancer-binding protein delta) is a transcription factor involved in cell growth, differentiation, inflammation, and metabolic processes, particularly in immune cells, adipocytes, hepatocytes, and fibroblasts.[20] However, the specific roles of GPD1 and CEBPD in MASLD and their potential as biological markers remain largely undefined.

In this study, we identified GPD1 and CEBPD as potential markers for MASH through bioinformatics analysis. We further validated their expression levels in animal models and cell-based experiments. Importantly, we investigated the biological function of GPD1 in MASH and found that it shows promise as a biological marker for this condition.

Method and Materials

Screening of Differentially Expressed Genes (DEGs)

The identification of differentially expressed genes (DEGs) distinguishing MASH from healthy controls was conducted utilizing the "limma" package in R. Genes meeting the threshold of an adjusted p-value below 0.05 and an absolute log2 fold change (FC) exceeding 0.3 were selected. Subsequently, the distribution and expression trends of the DEGs were illustrated through heatmaps and volcano plots.

Enrichment Analysis of DEGs

To explore the possible functions and biological significance of the identified DEGs, Gene Ontology (GO) and Kyoto Encyclopedia of Genes and Genomes (KEGG) enrichment analyses were performed. The enrichment process was

conducted using the "org. Hs.db", "clusterProfiler", "enrichplot", and "ggplot2" packages in R. Subsequently, the outcomes were depicted in bar plots, applying a significance threshold of p-value < 0.05.

Weighted Gene Co-Expression Network Analysis (WGCNA)

To determine gene modules strongly linked to MASH, weighted gene co-expression network analysis (WGCNA) was performed on the MerCohort using the R package "WGCNA". Outlier samples were eliminated through hierarchical clustering analysis, and the "pickSoftThreshold" function was applied to establish an optimal soft threshold ($\beta = 6$) for network formation. Genes exhibiting similar expression profiles were grouped into modules, and the module most closely associated with MASH was identified.

Discovery and Validation of Key Lipid Metabolism-Related Genes Associated with MASH

Key lipid metabolism-associated genes linked to MASH were identified by selecting those present across four categories: lipid metabolism-related genes, DEGs, and hub genes within the most relevant module detected through WGCNA. A Venn diagram was generated to illustrate the shared genes among these groups.

Machine Learning

The three machine learning algorithms primarily reference standard methods commonly used in conventional bioinformatics analyses.[21] As detailed in Supplementary Material 1.

Building of Nomogram and the Assessment of the Prediction Model

A clinically relevant nomogram was constructed using the two identified hub genes (CEBPD and GPD1) with the "rms" package in R. To assess its predictive performance for MASH, calibration curves were generated and analyzed.

Single-Sample Gene Set Enrichment Analysis (ssGSEA)

To comprehensively investigate immune cell infiltration patterns in MASH patients, the "GSVA" function in R was utilized to compute infiltration scores for each sample based on a predefined gene set of immune cell markers. Additionally, the Spearman correlation method was applied to assess relationships between immune cell infiltration and key genes.

Animal Experiments and Cells

All animal experiments received approval from the Taizhou Central Hospital Experimental Animal Welfare Ethics Committee, affiliated with Taizhou University. All procedures were conducted in strict accordance with relevant guidelines and regulatory standards. A total of 12 mice were used, with 6 mice in the MASH group and 6 mice in the normal group. The MASH animal model was established through high-fat diet feeding. XHF60 feed, sourced from SLAC Laboratory Animal Co., Ltd., was administered for 14 consecutive weeks. (XHF60 is a specialized high-fat diet for experimental animals, in which fat accounts for 60% of the total caloric intake. It is commonly used to establish metabolic liver disease models such as MASLD and MASH. The main components include fats, carbohydrates, and proteins, along with appropriate amounts of cellulose, vitamins, and minerals. In some protocols, cholesterol is added or combined with 10% fructose drinking water to enhance inflammatory or fibrotic phenotypes. The XHF60 diet reliably induces hepatic lipid accumulation, inflammatory responses, and metabolic disturbances, offering good reproducibility and clinical relevance). After collecting the animals' serum, it was sent to the Clinical Laboratory Department of Taizhou Central Hospital for analysis using an automated biochemical analyzer to measure transaminase, triglyceride, and cholesterol levels. HepG2 cells were purchased from Procell Life Science & Technology Co., Ltd., and cultured according to standard protocols. Lipid levels in the cell supernatant were measured using the ELISA method, with assay kits obtained from Solarbio Life Sciences. For detailed methods of insulin resistance assessment in mice, please refer to Supplementary Material 2.

RNA Interference and Gene Transfection

Small interfering RNAs (siRNAs) targeting GPD1, along with a scrambled control siRNA, were obtained from Wuhan Hewu Biotechnology Co., Ltd. The sequences of the GPD1 siRNAs were as follows: Si-1: 5′-GGAAGACAUUGGAGGCAAAtt-3′, 3′-UUUGCCUCCAAUGUCUUCCtt-5′; Si-2: 5′-GGAAAGUGGCUGAGGCCUUtt-3′, 3′-AAGGCCUCAGCCACUUUCCtt-5′; Si-3: 5′-GCAGAAUCAUCCAGAACAUtt-3′, 3′-AUGUUCUGGAUGAUUCUGCtt-5′. Transfection of GPD1 siRNAs into Hepa1-6 cells was carried out using Lipofectamine 2000 (Invitrogen, Green Island, CA), following the manufacturer's instructions. The overexpression sequence of CEBPD is detailed in Supplementary Material 3.

Oil Red O Staining

HepG2 cells were plated in 6-well dishes and cultured until reaching approximately 80% confluence. Following treatment, the cells were rinsed with PBS, fixed in 4% paraformaldehyde for 30 minutes, and stained with Oil Red O solution for 15 minutes. Excess dye was removed using 60% isopropanol. Lipid droplet accumulation was observed using an inverted microscope (IX51, Olympus, Japan), and staining intensity was quantified by extracting the dye with isopropanol and measuring absorbance at 510 nm. All experiments were conducted in triplicate to ensure reproducibility.

Quantitative Polymerase Chain Reaction (qPCR) and Western Blotting (WB)

After collecting the cells, RNA was extracted, and its quality was verified. The RNA was then reverse-transcribed into cDNA, followed by qPCR analysis performed on a Bio-Rad PCR instrument according to the reagent kit's instructions. The primer sequences used are as follows: β-actin: Forward: 5′-CACCATTGGCAATGAGCGGTTC-3′, Reverse: 5′-AGGTCTTTGCGGATGTCCACGT-3′; TNF-α: Forward: 5′-CAGCCTCTTCTCCTTCCTGAT-3′, Reverse: 5′-GCCAGAGGGCTGATTAGAGA-3′; IL-6: Forward: 5′-ACTCACCTCTTCAGAACGAATTG-3′, Reverse: 5′-CCATCTTTGGAAGGTTCAGGTTG-3′; TGF-β: Forward: 5′-TGAGTGGCTGTCTTTTGACG-3′ Reverse: 5′-TGGTTGTAGAGGGCAAGGAC-3′.

Proteins were extracted from the liver tissues of normal and MASLD mice and separated using 10% SDS-PAGE. After adjusting the sample loading volumes, WB analysis was conducted to evaluate the expression levels of GPD1 and CEBPD. The GPD1 antibody was obtained from Proteintech, while the CEBPD antibody was sourced from Abmart. Tubulin, purchased from Abways, was used as the internal control. Antibody dilutions were prepared following the manufacturer's instructions. Grayscale values were analyzed using ImageJ software after imaging, and all experiments were performed in triplicate.

Immunohistochemistry (IHC) AND Hematoxylin and Eosin Staining (H&E)

Tissues were fixed in paraformaldehyde and embedded to prepare paraffin sections. Following dehydration, experiments were conducted according to the requirements for HE staining and IHC. The antibodies used for IHC were the same as those used in the WB experiments. After successful staining, images were acquired via scanning and analyzed for average optical density (AOD) using ImageJ software.

Statistics

Statistical analyses were performed using R software (Version 4.2.3) and GraphPad Prism (Version 9.3.2). Comparisons between the two groups were conducted using either unpaired Student's *t*-tests or Wilcoxon tests, depending on data distribution. Relationships between hub genes and immune cell infiltration were examined using Spearman correlation analysis. A p-value below 0.05 was regarded as statistically significant.

Result

Data Preprocessing and Batch Effect Correction

Initially, data were obtained from three GEO datasets (GSE164760, GSE48452, and GSE89632), which contained bulk RNA sequencing profiles from both healthy individuals and MASH patients (Figure 1A). To enhance accuracy and

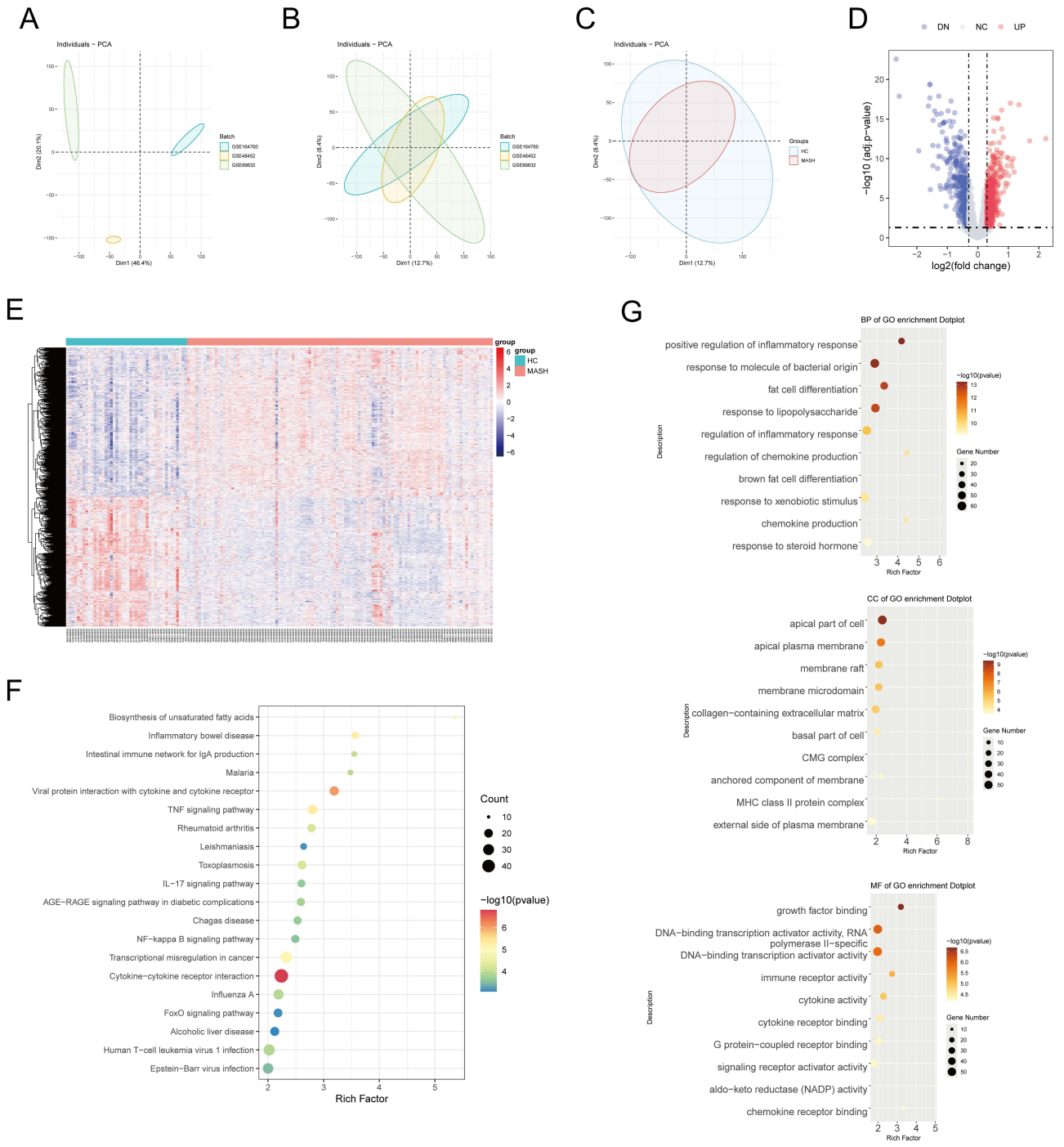

Figure 1 Functional enrichment analysis in healthy controls and patients with MASH groups. PCA analysis shows the distribution of samples in GSE164760, GSE48452, and GSE89632 before (**A**) and after (**B**) batch effect correction. (**C**) PCA analysis shows the distribution of samples in healthy controls and patients with MASH. (**D**) Volcano plots showing the DEGs between patients with MASH and healthy controls. (**E**) Illustration of DEGs in MerCorhort using the heatmap. KEGG (**F**) and GO (**G**) analysis between patients with MASH and healthy controls.

reliability, batch effect correction was applied before merging the datasets, yielding a combined cohort consisting of 44 healthy controls and 111 MASH patients (Figure 1B). PCA indicated that the patients with MASH were notably distinct from the healthy controls (Figure 1C).

https://doi.org/10.2147/JIR.S524204

Functional Enrichment Analysis in Healthy Controls and Patients with MASH Groups

A filtering strategy was applied to identify differentially expressed genes (DEGs), selecting those with an adjusted p-value < 0.05 and an absolute log2 fold change (FC) greater than 0.3 (Figure 1D and E). KEGG analysis highlighted the enrichment of pathways linked to unsaturated fatty acid biosynthesis and inflammation- and immunity-related signaling, including the TNF-α and IL-17 signaling pathways, as well as cytokine-cytokine receptor interactions. (Figure 1F). Similarly, GO analysis identified significant enrichment of pathways associated with adipocyte differentiation, inflammatory responses, extracellular matrix remodeling, fibrosis, and growth factor binding in the MASH group (Figure 1G).

WGCNA to Identify Hub Modules and Hub Genes Associated with MASH

WGCNA was conducted to identify key modules and hub genes associated with MASH. Clustering analysis revealed no outlier samples in the dataset (Figure 2A). A soft threshold power (β) of 6 was chosen based on the scale-free topology model fit and mean connectivity (Figure 2B). Subsequently, network construction and module identification resulted in 14 gene co-expression modules (Figure 2C). An eigengene adjacency heatmap was generated to illustrate correlations between modules (Figure 2D). Among the six identified modules, the yellow and green modules exhibited the strongest associations with MASH ($R = 0.37$ and -0.68, $p < 0.001$) (Figure 2E). These two modules were designated as hub modules, and hub genes were selected based on MM > 0.7 and GS > 0.25 (Figure 2F and G).

Nutrients and metabolites are essential regulators of immune cell function. When activated, immune cells undergo metabolic reprogramming to accommodate heightened energy requirements and sustain immune responses.[22] The interplay between metabolism and immune cells shapes both innate and adaptive immunity. To explore these dynamics, we analyzed the metabolic pathway profiles of the MASH and healthy control groups. Our analysis revealed alterations in multiple metabolic pathways in the MASH group, including classical energy metabolism pathways such as the citric acid cycle, fatty acid degradation, and glycogen degradation. Notably, Lipid metabolism pathways exhibited high activity in the MASH group. Recent research has highlighted the crucial role of lipids in mammalian immune regulation, especially in inflammation, though the underlying mechanisms remain a subject of debate.[23] Therefore, we focused on lipid metabolism for further investigation. To identify key lipid metabolism associated with MASH, we intersected DEGs. To pinpoint key lipid metabolism-associated genes linked to MASH, we identified the intersection of DEGs, hub genes, and lipid metabolism-related genes, yielding 13 key candidates (Figure 3A). A correlation analysis was conducted, and a heatmap was generated based on the complete expression matrix of these 13 genes in the MerCohort (Figure 3B). Among them, PTGS2, CEBPD, and KLF4 exhibited significant negative correlations with the remaining 10 genes.

Consensus Clustering of Lipid Metabolism-Related Genes

To gain a comprehensive understanding of how lipid metabolism-related gene expression influences MASH, we conducted consensus clustering analysis to identify lipid metabolism subtypes. This analysis classified MASH patients in the MerCohort into two distinct subtypes, designated as subtype 1 and subtype 2 (Figure 3C and D). Principal component analysis (PCA) further confirmed that these subtypes were effectively distinguishable (Figure 3E). Additionally, heatmap and volcano plot analyses revealed significant differences in gene expression profiles between the two subtypes (Figure 3F and G). To further investigate the expression patterns of lipid metabolism-related genes in subtypes 1 and 2, a differential expression analysis was conducted. The findings revealed that ACAA1, ACBD4, CEBPA, GPAM, GPD1, MOGAT2, MTMR4, PRKAB2, SLC25A1, and THRSP were significantly upregulated in subtype 1. Conversely, in subtype 2, CEBPD, KLF4, and PTGS2 exhibited higher expression levels (Figure 3H).

Beyond analyzing the overall distribution of lipid metabolism-related genes, we further examined the functional enrichment differences between subtype 1 and subtype 2 in greater detail. By GSVA analysis, we performed GO and KEGG enrichment analysis of these two isoforms. GO enrichment analysis revealed significant associations with fatty acid metabolism, fatty acid oxidation, lipid catabolic processes, and fatty acid derivative metabolic pathways (Figure 4A). Similarly, KEGG enrichment analysis identified pathways related to fatty acid metabolism (Figure 4B).

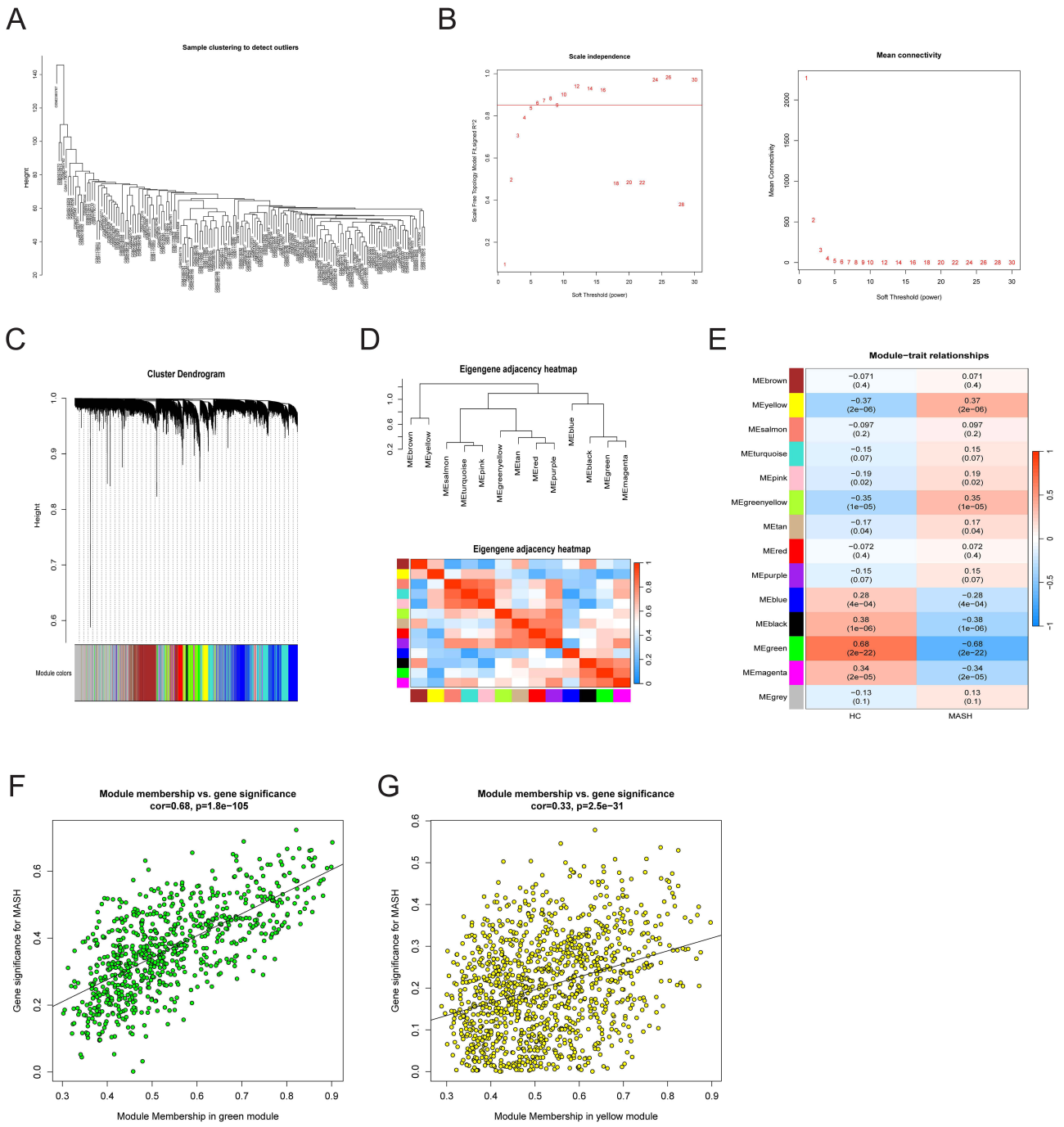

Figure 2 WGCNA to identify hub modules and hub genes associated with MASH. (**A**) Dendrogram of sample clustering. (**B**) Determination of soft threshold power for MerCorhort. (**C**) Cluster dendrogram of MASH highly connected genes in key modules. (**D**) Eigengene adjacency heatmap showing the correlation between every two modules. (**E**) Heatmap of the correlation between each module and trait. Red and blue indicate a positive or negative correlation, respectively. The darker the color, the stronger the correlation. Scatter plot of the relationship between module membership and gene significance in green (**F**) and yellow (**G**) modules. Genes in the right upper quadrant are identified as hub genes.

Immune Infiltration and Differential Gene Analysis of Subtypes 1 and 2

Immuno-infiltration analysis revealed significant differences in immune cell infiltration levels between subtypes 1 and 2, with subtype 1 exhibiting a lower proportion of infiltrating immune cells compared to subtype 2 (Figure 4C). Notably, CD56bright natural killer cells, gamma delta T cells, immature B cells, and memory B cells were predominantly enriched in subtype 1, whereas MDSCs, $CD4^+$ activated T cells, $CD8^+$ activated T cells, and monocytes were more abundant in

https://doi.org/10.2147/JIR.S524204

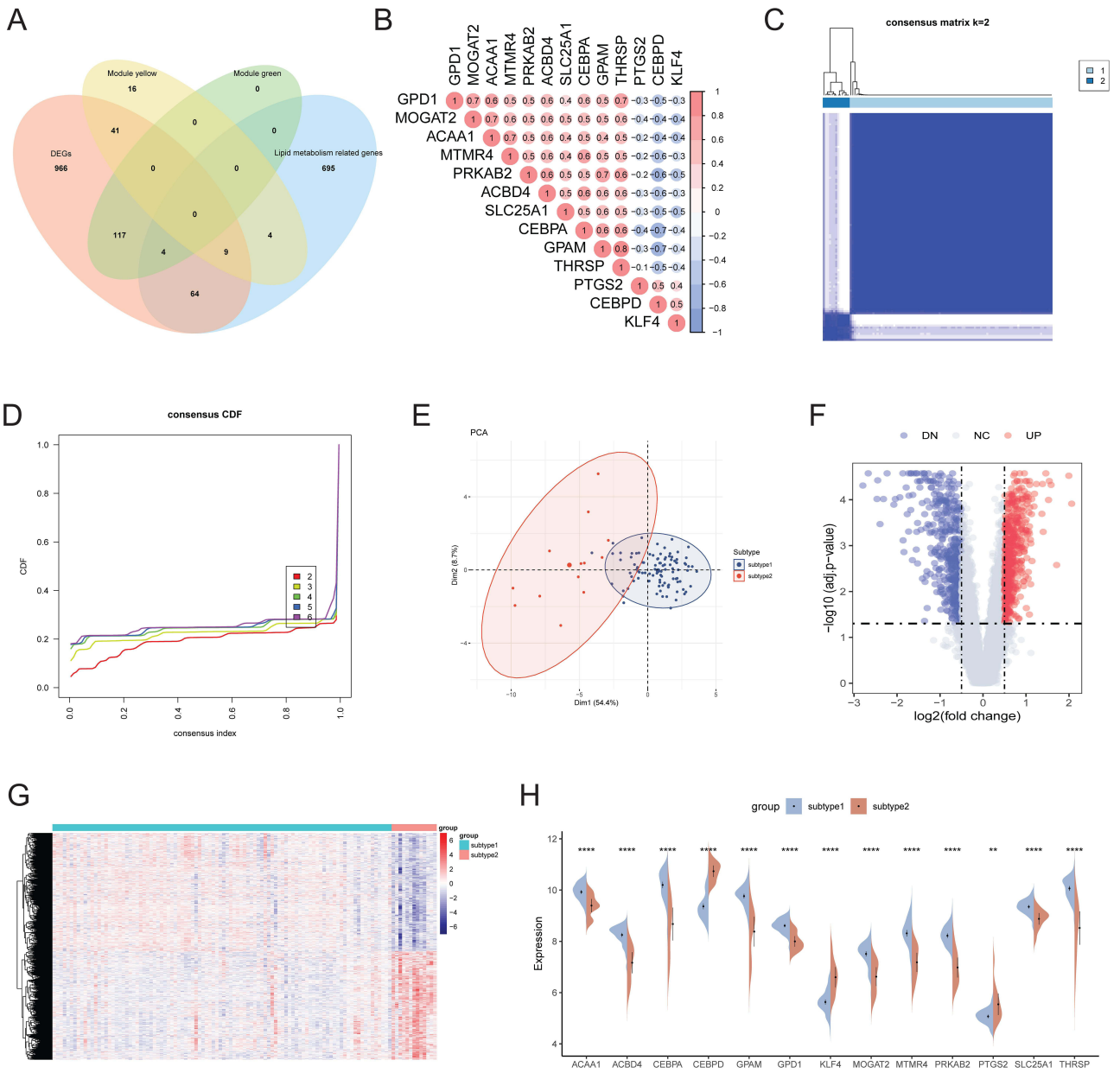

Figure 3 Consensus clustering of lipid metabolism-related genes. (**A**)Venn diagram of the overlap among DEGs, hub genes in the yellow module, hub genes in the green module, and lipid metabolism-related genes. (**B**) The correlation analysis between hub genes. The darker the color, the stronger the correlation. (**C**). Consensus clustering matrix for k = 2. (**D**) Consensus CDF curves for k = 2 to 6. (**E**) PCA of two subtypes. (**F**) Volcano plots showing the DEGs between two subtypes. (**G**) Illustration of DEGs between two subtypes using the heatmap. (**H**) The split violin plot showed the expression of 13 lipid metabolism-related genes between the two subtypes. $^{**}p \leq 0.001$, $^{****}p \leq 0.0001$.

subtype 2 (Figure 4D). Additionally, ssGSEA analysis confirmed that all 13 fatty acid metabolism-related genes play a role in regulating immune cell function (Figure 4E).

Identification of Shared Hub Genes Using Machine Learning Algorithms

To identify potential diagnostic biomarkers, machine learning algorithms were applied to screen the 13 key genes. Based on the variable importance analysis, the final set of characteristic genes was identified by selecting the top three genes common to LightGBM, SVM-REF, and Random Forest: CEBPD and GPD1 (Figure 5).

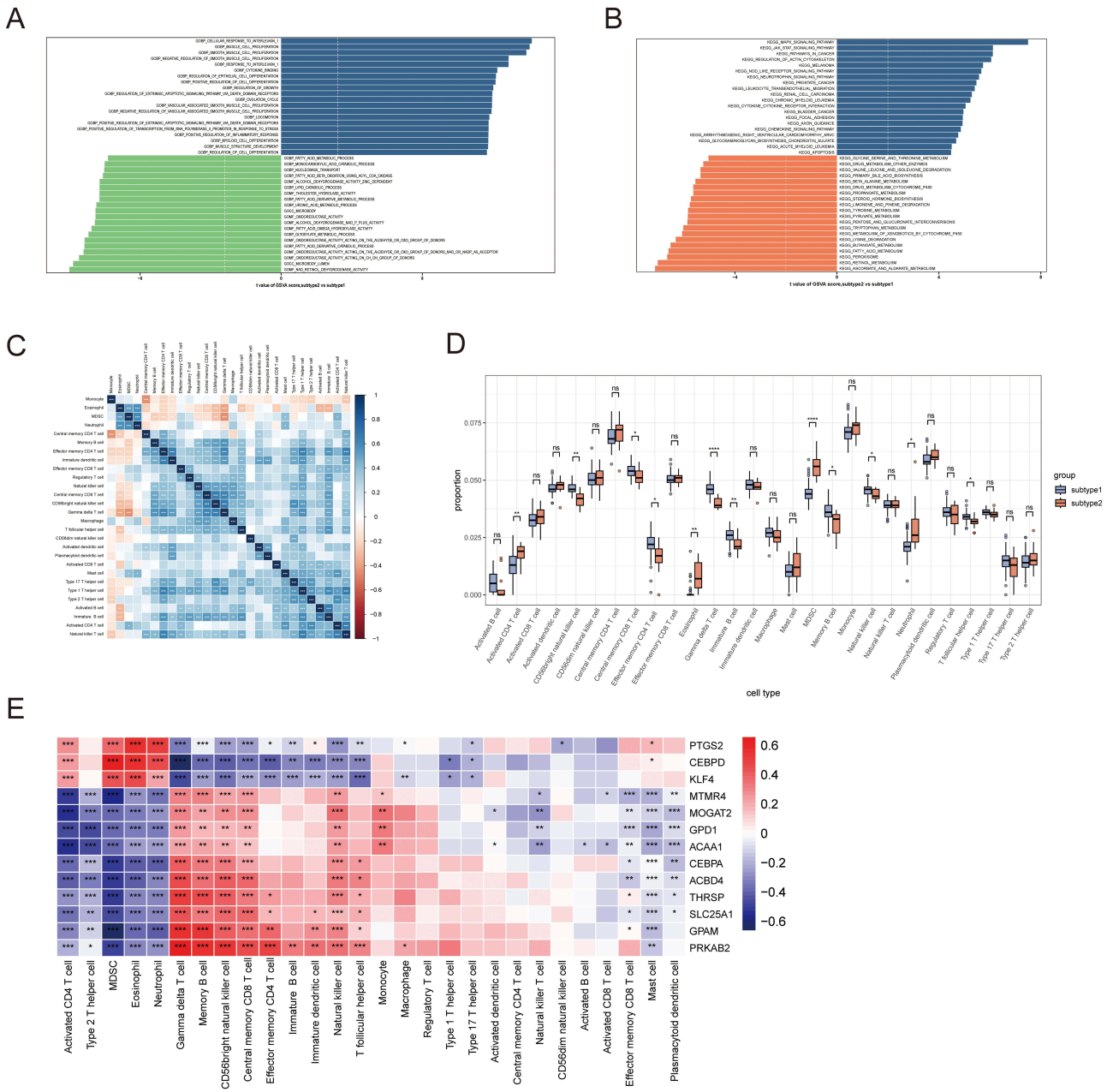

Figure 4 Immune infiltration and differential gene analysis of subtypes 1 and 2. Differences in enriched biological functions (**A**) and hallmark pathways (**B**) between subtypes, ranked by GSVA scores. (**C**) Heatmap showing correlations between 28 immune cell types. (**D**) Boxplot depicting differences in immune cell infiltration between subtypes. (**E**) Heatmap showing the correlation between 13 lipid metabolism-related gene expression and immune cells in MASH. * $p < 0.05$, ** $p < 0.01$, *** $p < 0.001$, **** $p < 0.0001$, ns not significant ($p \geq 0.05$).

Construction of Nomogram and Clinical Risk Prediction

A nomogram was developed based on the two identified hub genes, and a calibration plot was generated to assess the model's predictive performance (Figure 6A). The calibration plot demonstrated minimal deviation between the observed event risk and the predicted event risk, indicating the model's reliability (Figure 6B). A DCA plot was constructed to evaluate the clinical applicability of the diagnostic model based on the selected genes (Figure 6C). The model's curve remained stable within a defined range and consistently outperformed both the all-positive and all-negative scenarios. This demonstrated a higher net benefit, highlighting the model's strong predictive performance. ROC curves of linear predictors for the logistic regression models in different groups also revealed good diagnostic effects (Figure 6D). The

https://doi.org/10.2147/JIR.S524204

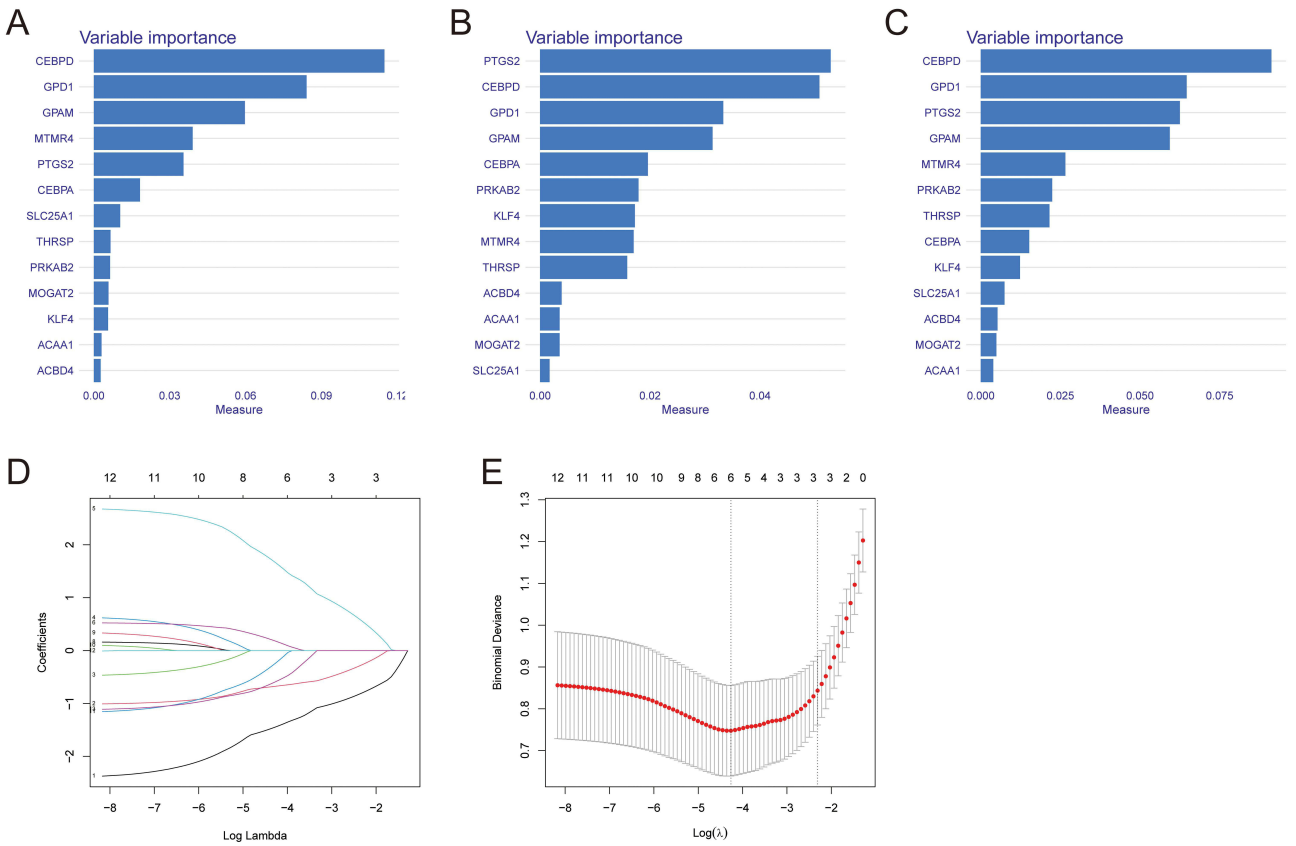

Figure 5 Identify potential diagnostic biomarkers from 13 key genes. Variable importance plot in LightGBM (**A**), SVM-REF (**B**), and Random Forest (**C**). (**D**) Plot of variable trajectories of the LASSO diagnostic model. (**E**) A diagram illustrating the LASSO regression diagnostic model for lipid metabolism-related genes in MASH.

risk score derived from the model showed significant variation between patients with MASH and healthy controls in the training set (Figure 6E). Next, the GSE213621 dataset was utilized for external validation. Results indicated a significant difference in the risk scores generated by the model between MASH patients and healthy controls in the test set (Figure 7A). Receiver operating characteristic (ROC) analysis further confirmed the nomogram's strong diagnostic capability, achieving an AUC of 0.773 (Figure 7B).

Identification and Verification of the Key Lipid Metabolism-Related Genes Associated with MASH

The expression levels of key genes were validated in the MerCohort by comparing healthy controls and MASH patients. Receiver operating characteristic (ROC) curve analysis demonstrated that CEBPD and GPD1 possessed significant clinical diagnostic value for MASH (Figure 7C and D). Further validation using the GSE213621 dataset confirmed these findings, showing a progressive increase in GPD1 expression in MASH patients, while CEBPD exhibited a sequential decline compared to healthy controls (Figure 7E). Additionally, ROC analysis reinforced the potential of these key genes as biomarkers for MASH diagnosis (Figure 7F and G). The relationship between key gene expression and fibrosis stage was further examined using the GSE213621 dataset. As shown in Figure 7H and I, CEBPD and GPD1 were significantly downregulated in the F2 and F3F4 groups compared to the F0F1 group among MASH patients. These findings suggest that CEBPD and GPD1 exhibit marked downregulation during the early and moderate stages of MASH progression.

These findings indicate that CEBPD and GPD1 may serve as potential biomarkers for MASH. To further investigate immune cell differences between MASH patients and healthy controls, the ssGSEA algorithm was applied. Figure 8A illustrates the correlations among 28 immune cell types, revealing a negative correlation between central memory T cells and

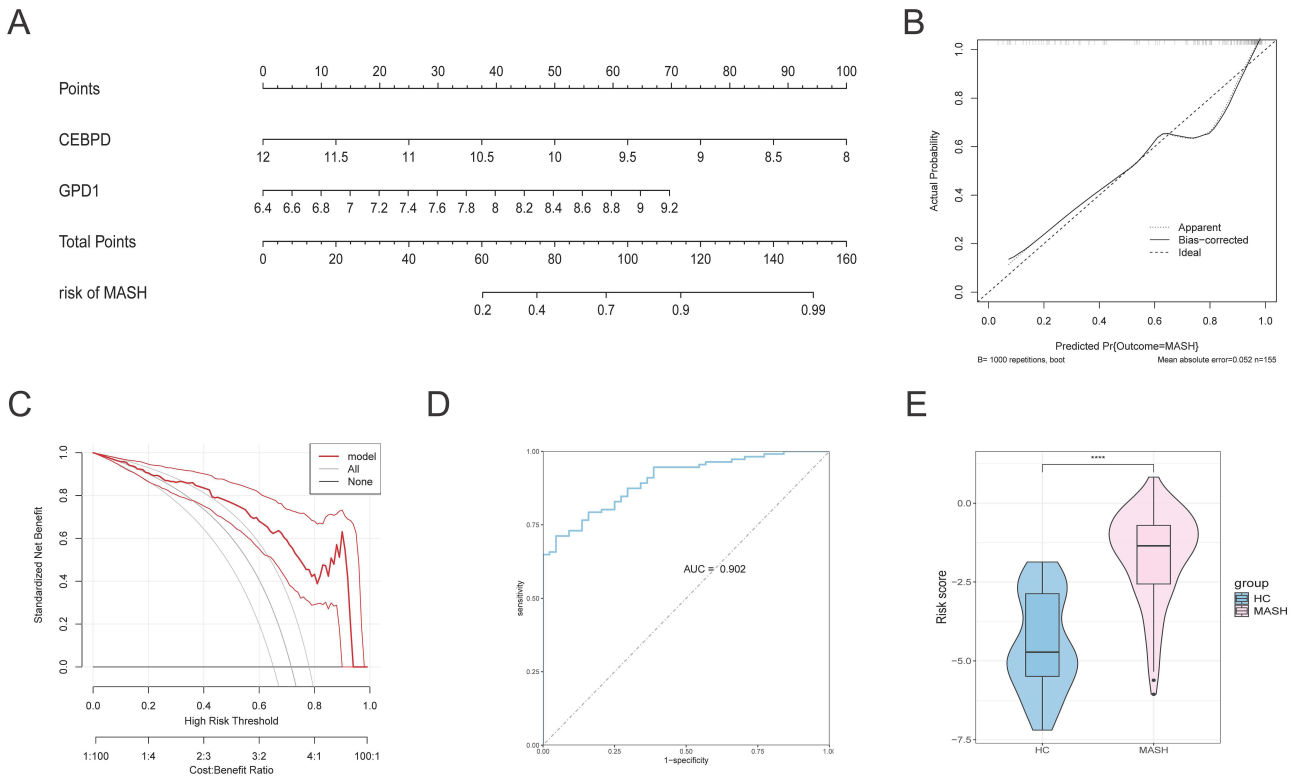

Figure 6 Construction of Nomogram and Prediction of Clinical Risk. (**A**) The nomogram was visualized using 2 candidate biomarkers to predict the risk of MASH. Construction of calibration curve (**B**) and DCA (**C**) to evaluate the predictive efficiency of the nomogram model in the train set. (**D**) ROC curves assessed the model's diagnostic performance in the training set. (**E**) Comparison of risk distributions between patients with MASH and healthy controls in the train set. **** $p < 0.0001$.

monocytes (R = −0.6) and a positive correlation between activated $CD4^+$ T cells and natural killer T cells (R = 0.59). Furthermore, natural killer T cells displayed negative correlations with both monocytes (R = −0.61) and eosinophils (R = −0.51). Finally, we compared the immune cell infiltrations and immune functions between the groups, as shown in Figure 8B and C. Immune cell infiltration and the activation of various immune functions were analyzed to explore their roles in MASH pathogenesis. The results revealed distinct differences in immune cell distribution and functional activation between MASH patients and healthy controls, highlighting potential immunological mechanisms underlying disease progression, and a heat map showing the correlation between CEBPD and GPD1 expression and immune cells in MASH (Figure 8D).

Validation of the Role of CEBPD and GPD1 in Inflammation in vitro and vivo Models

Animal models of MASH were established, and HE staining revealed significant ballooning degeneration and MASLD-like features in the MASH group (Figure 9A and B). Serum liver function markers, triglyceride levels, and total cholesterol levels were significantly elevated in the MASH group compared to the CON group (Figure 9C–F). Similarly, the body weight, liver weight, and liver index were markedly elevated in the MASH group (Figure 9G–I).

To evaluate insulin resistance in the MASH mouse model, fasting blood glucose (FBG) and fasting insulin (FINS) levels were measured, and HOMA-IR and QUICKI indices were calculated. As shown in Figure S1, MASH mice exhibited significantly higher FBG and FINS compared with normal mice. Meanwhile, HOMA-IR was markedly increased, and QUICKI was significantly decreased in MASH mice. These results indicate that high-fat diet–induced MASH mice display pronounced insulin resistance compared with age-matched controls.

Immunohistochemistry confirmed that GPD1 expression was significantly upregulated, while CEBPD expression was notably downregulated in the MASH group relative to the CON group (Figure 10A–C). These findings were further validated by Western blot analysis (Figure 10D–F). Given the greater clinical utility of positive expression markers over

https://doi.org/10.2147/JIR.S524204

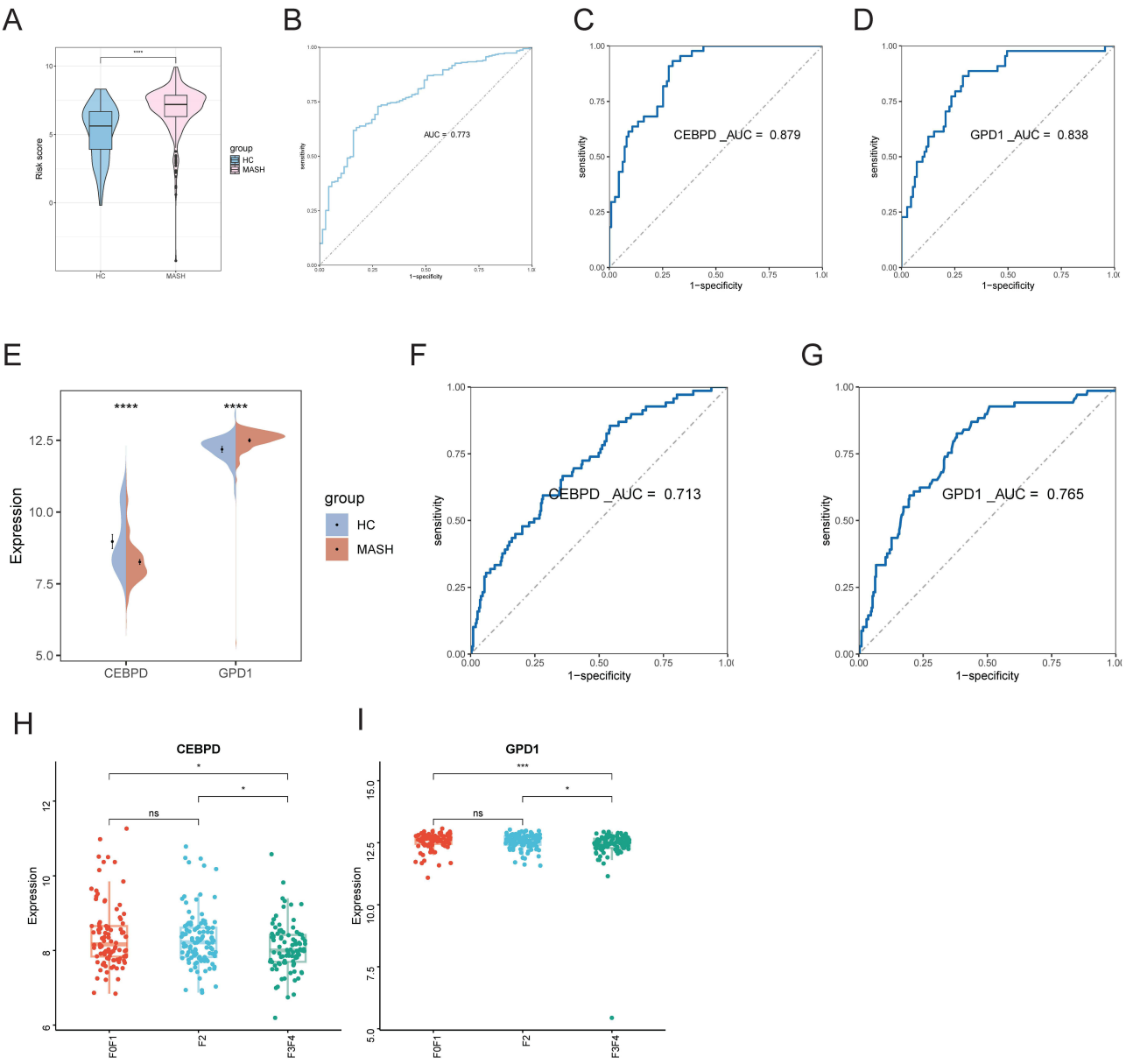

Figure 7 Diagnostic Performance and Clinical Relevance of CEBPD and GPD1 in MASH Patients. (**A**) Comparison of risk distributions between patients with MASH and healthy controls in the test set. (**B**) ROC curves assessed the model's diagnostic performance in the test set. ROC curves assessed the diagnostic performance of CEBPD (**C**) and GPD1 (**D**) in the train set. (**E**) Comparison of CEBPD and GPD1 expression levels between patients with MASH and HC in the test set. ROC curves evaluated the diagnostic performance of CEBPD (**F**) and GPD1 (**G**) in the test set. (**H** and **I**) The association between the expression level of CEBPD and GPD1 and the fibrosis stage. * $p < 0.05$, *** $p < 0.001$, **** $p < 0.0001$, ns not significant ($p \geq 0.05$).

negative markers for disease diagnosis, the role of GPD1 in MASH was further examined using a cellular model. Fatty acid stimulation significantly increased GPD1 expression in HepG2 cells. The knockdown efficiency of three siRNAs targeting GPD1 was assessed using qPCR and Western blotting (Figure 11A and B). Among them, siGPD1#1 and siGPD1#2 exhibited the highest silencing efficiency and were selected for further experiments. Oil Red O staining demonstrated that GPD1 knockdown markedly suppressed fatty acid-induced lipid accumulation (Figure 11C). Moreover, the fatty acid-induced upregulation of TC, TG, IL-6, TGF-β, and TNF-α was inhibited following GPD1 knockdown (Figure 11D), indicating the potential anti-inflammatory and anti-MASH roles of GPD1.

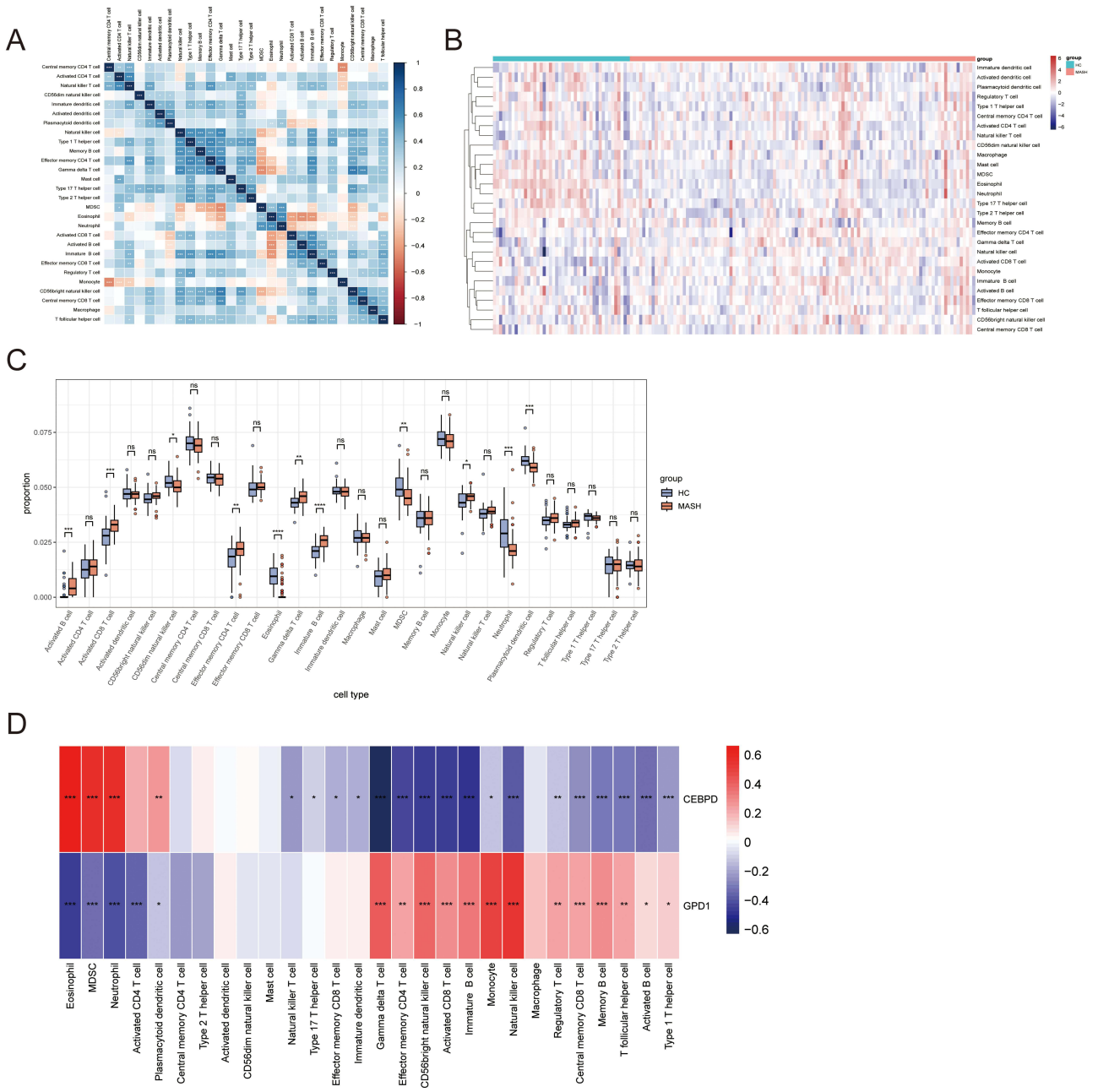

Figure 8 Immune Cell Profiling and Correlation with CEBPD and GPD1 Expression in MASH. (**A**) Heatmap showing correlations between 28 immune cell types in MerCorhort. (**B**) Heatmap showing the infiltrating enrichment of 28 immune cell types in MerCorhort. (**C**) Boxplot depicting differences in immune cell infiltration between patients with MASH and healthy controls. (**D**) Heatmap showing the correlation between CEBPD and GPD1 expression and immune cells in MASH. * $p < 0.05$, ** $p < 0.01$, *** $p < 0.001$, **** $p < 0.0001$, ns not significant ($p \geq 0.05$).

Meanwhile, we further supplemented the functional experiments for CEBPD. Fatty acid stimulation significantly downregulated CEBPD expression in HepG2 cells. The overexpression efficiency of three plasmids targeting CEBPD was evaluated using qPCR and Western blotting (Figure S2A and S2B), among which OeCEBPD#2 and OeCEBPD#3 exhibited the highest overexpression efficiency and were selected for subsequent experiments. Oil Red O staining showed that CEBPD overexpression markedly inhibited fatty acid-induced lipid accumulation (Figure S2C). Moreover, the fatty acid-induced elevations in TC, TG, IL-6, TGF-β, and TNF-α levels were significantly suppressed following CEBPD overexpression (Figure S2D).

https://doi.org/10.2147/JIR.S524204

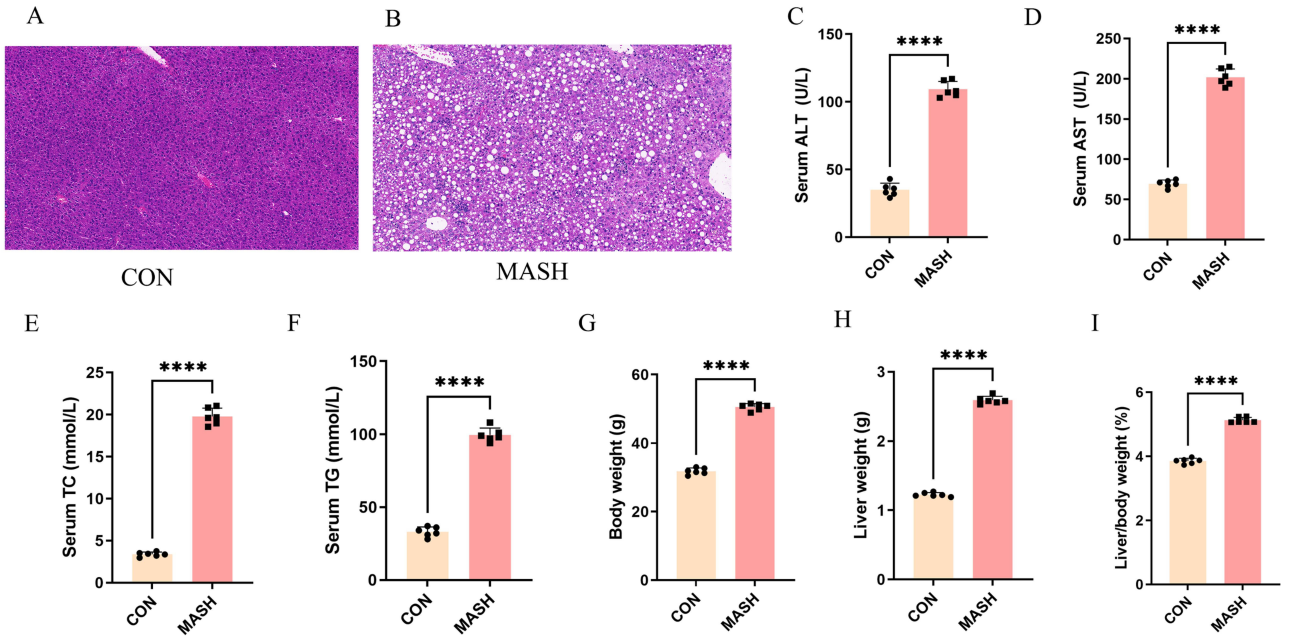

Figure 9 Successfully established the animal model of MASH. (**A**) H&E staining of normal liver tissue (n=6), 400×, scale bar 100 μm. (**B**) H&E staining of MASH liver tissue (n=6), 400×, scale bar 100 μm. (**C**) Comparison of ALT levels between CON and MASH groups. (**D**) Comparison of AST levels between CON and MASH groups. (**E**) Comparison of TC levels between CON and MASH groups. (**F**) Comparison of TG levels between CON and MASH groups. (**G**) Comparison of body weight between CON and MASH groups. (**H**) Comparison of liver weight between CON and MASH groups. (**I**) Comparison of liver index between CON and MASH groups. **** $p \leq 0.0001$.

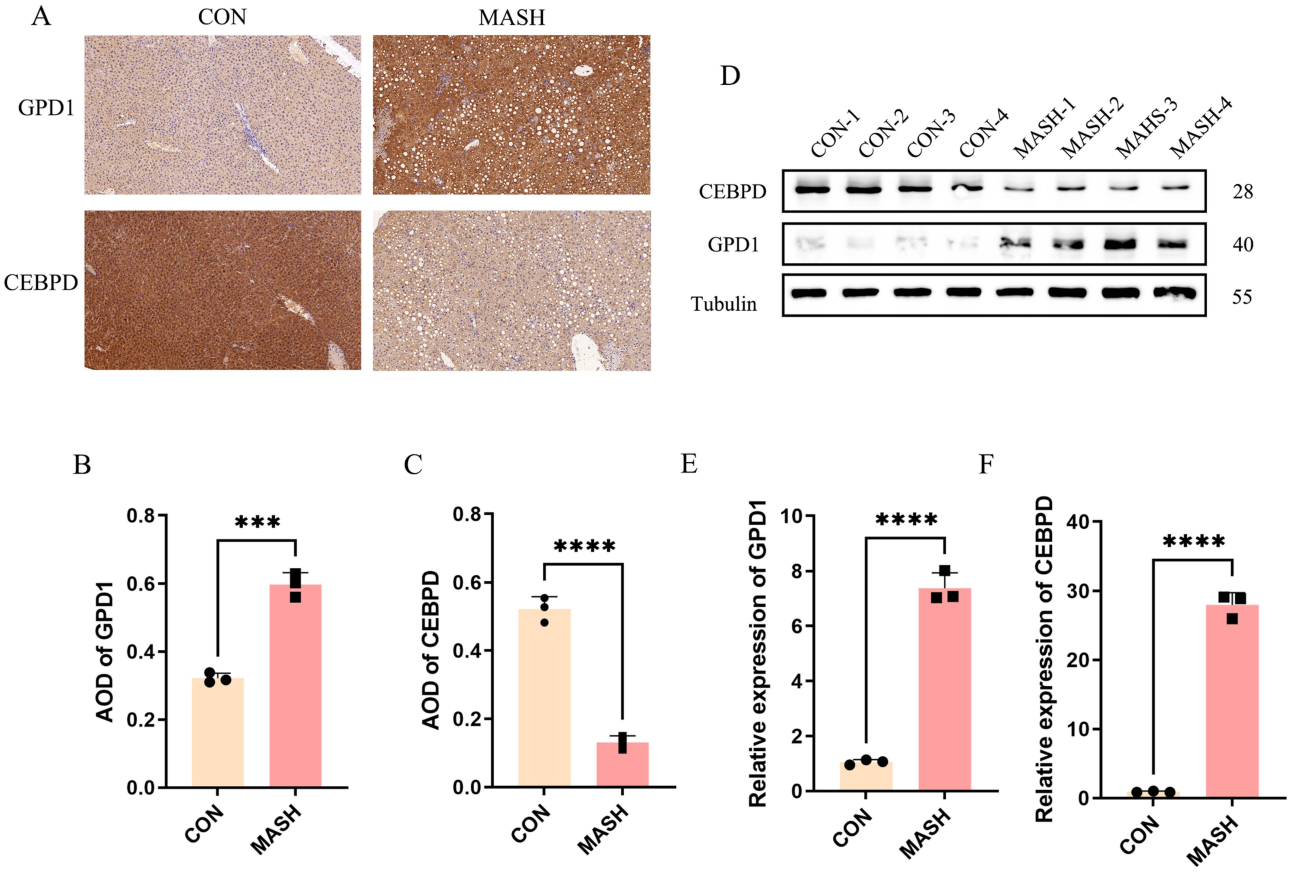

Figure 10 Validation of GPD1 and CEBPD in a MASH Animal Model. (**A**) IHC staining of normal and MASH liver tissues, n = 6, 400×, scale bar 100 μm. (**B**) AOD values for GPD1 in CON and MASH groups. (**C**) AOD values for CEBPD in CON and MASH groups. (**D**) WB analysis of normal and MASH liver tissues, n = 3. (**E**) Relative gray value measurements for GPD1 in CON and MASH groups. (**F**) Relative gray value measurements for CEBPD in CON and MASH groups. ***$p \leq 0.001$.****$p \leq 0.0001$.

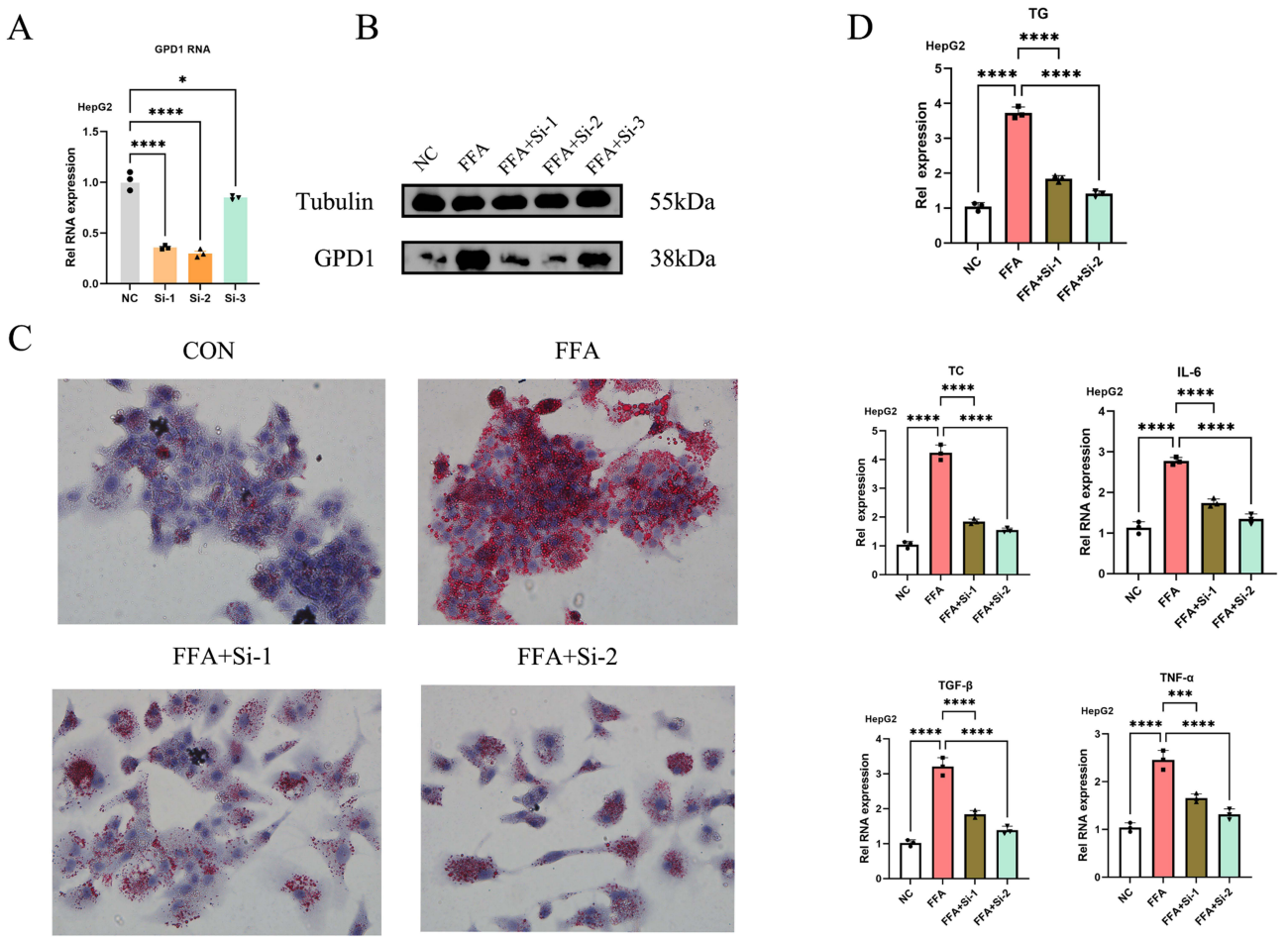

Figure 11 Effects of GPD1 Knockdown on Lipid Accumulation and Inflammatory Mediator Expression in HepG2 Cells. (**A**) QPCR analysis confirming the knockdown efficiency of three siRNAs targeting GPD1 in HepG2 cells. Statistical markers represent a comparison between the NC group and the other groups. (**B**) WB validating the knockdown efficiency of GPD1 by the three siRNAs. (**C**) Oil Red O staining demonstrates that GPD1 knockdown markedly suppresses fatty acid-induced lipid accumulation in HepG2 cells. (**D**) Quantification of TG, TC, and pro-inflammatory cytokines (IL-6, TGF-β, and TNF-α) shows that GPD1 knockdown inhibits fatty acid-induced upregulation of these molecules. Statistical markers represent a comparison between the FFA group and the other groups * $p \leq 0.05$, *** $p \leq 0.001$, ****$p \leq 0.0001$.

Taken together, these findings indicate that GPD1 and CEBPD may serve as novel biomarkers and potential therapeutic targets for MASH.

Discussion

This study combined bioinformatics with in vitro and in vivo experiments to comprehensively investigate the role of lipid metabolism-related genes in MASH. Our findings highlight CEBPD and GPD1 as potential biomarkers and therapeutic targets for MASH. Notably, while CEBPD is downregulated, GPD1 is significantly upregulated in MASH. Furthermore, we confirmed that knockdown of GPD1 and overexpression of CEBPD can effectively suppress the progression of MASH. Overall, this study offers new perspectives on the molecular mechanisms of MASH, particularly the contributions of fatty acid metabolism-related genes.

Metabolic disorders, particularly lipid metabolism dysregulation leading to insulin resistance and abnormal lipid deposition, are hallmark features of MASLD.[24] Our findings revealed significant lipid metabolism dysregulation in MASH patients. Differential expression analysis, combined with WGCNA and functional enrichment analyses, identified pathways such as fatty acid metabolism, lipid oxidation, and catabolism as significantly enriched in the MASH group. Notably, lipid metabolism-related genes exhibited distinct expression profiles between subtype 1 and subtype 2, highlighting the heterogeneity of lipid metabolism in MASH. This also explains the complexity and diversity of MASLD and

https://doi.org/10.2147/JIR.S524204

MASH driven by lipid dysregulation. These findings align with prior studies, underscoring the critical role of lipid dysregulation in driving inflammation and fibrosis in metabolic liver diseases.[25–28]

The interplay between lipid metabolism and immune cell function was a central theme of our analysis. Immune infiltration analysis further confirmed significant differences between subtypes, with subtype 1 exhibiting lower immune cell infiltration compared to subtype 2. Certain immune cell populations, including CD56bright natural killer cells and memory B cells, play a significant role in MASH-related immune responses, and were predominantly enriched in subtype 1, whereas MDSCs and activated T cells were enriched in subtype 2. These findings suggest that lipid metabolism influences immune cell recruitment and activation, potentially driving the pathogenesis of MASH through immune-mediated mechanisms.[22,29] Lipid metabolism exerts a significant influence on immune cell function, recruitment, and activation. The interaction between lipid metabolism and immune cells not only drives inflammatory responses but also promotes fibrosis progression in MASH. Activated immune cells release profibrogenic mediators that stimulate hepatic stellate cells to produce extracellular matrix. Additionally, chronic activation of immune cells exacerbates oxidative stress and endoplasmic reticulum stress, further damaging hepatocytes and advancing the progression of MASH.[30,31]

Moreover, dysregulated fatty acid metabolism is not only a key metabolic feature of MASH but also a major contributor to immune cell infiltration. Excessive free fatty acids can activate inflammatory pathways such as TLR4/NF-κB, inducing Kupffer cells to release pro-inflammatory cytokines, including IL-1β and TNF-α, thereby promoting the recruitment and activation of immune cells.[32,33] In addition, lipid metabolism–related genes such as SREBP-1c and PPARγ play crucial roles in regulating triglyceride synthesis, oxidative stress, and macrophage polarization, providing mechanistic evidence supporting a causal link between lipid metabolic imbalance and immune dysregulation.[34,35] Our findings also suggest a significant correlation between the abnormal expression of lipid metabolism genes and the infiltration levels of $CD4^+$ T cells, MDSCs, and NK cells. Therefore, lipid metabolic disturbances may play a central regulatory role in reshaping the hepatic immune microenvironment and driving the progression of inflammation and fibrosis in MASH.

Machine learning algorithms identified CEBPD and GPD1 as the most reliable diagnostic biomarkers for MASH. ROC curve analysis confirmed their significant diagnostic performance in both the training and external validation cohorts. Notably, CEBPD and GPD1 exhibited contrasting expression patterns in MASH patients, with CEBPD down-regulated and GPD1 upregulated. Moreover, their expression levels were associated with fibrotic stages, indicating their potential roles in MASH progression. As a key regulator of lipid metabolism, GPD1 has been implicated in diverse functions. While some studies suggest that innate GPD1 deficiency may result in hepatic steatosis and fibrosis, this underscores the multifaceted roles of GPD1 in lipid metabolism.[36] Consequently, MASH-targeted therapies involving GPD1 require further rigorous investigation to establish their therapeutic potential.[37]

Functional experiments provided robust evidence for the pro-inflammatory and pro-MASH roles of GPD1. In vitro studies revealed that fatty acid stimulation significantly upregulated GPD1 expression, promoting lipid accumulation and elevating levels of pro-inflammatory mediators. Knockdown of GPD1 effectively suppressed these effects, underscoring its pivotal role in lipid-induced inflammation. Similarly, in vivo experiments validated the upregulation of GPD1 in MASH animal models, reinforcing its potential as a therapeutic target. In addition to directly regulating lipid metabolism and associated immune and inflammatory responses, GPD1 contributes to the pro-inflammatory and pro-fibrotic micro-environment of MASH.[38,39] Moreover, GPD1 may serve as a key node in the interplay of multiple factors driving MASH pathogenesis.[40] In metabolic diseases, GPD1 is regulated by the glucocorticoid receptor and can promote bladder cancer progression by mediating the cell cycle pathway.[41] Additionally, GPD1 can regulate HIF1α, affecting mitochondrial function and contributing to renal cancer development,[17] indicating a close relationship between GPD1 and metabolic disorders.

Strengths and Limitations of the Study

This study presents several notable strengths. By systematically integrating bioinformatics analyses with both in vivo and in vitro experiments, we comprehensively investigated the roles of lipid metabolism–related genes in the pathogenesis of MASH. The use of multiple machine learning algorithms—including WGCNA, LASSO, RF, and SVM-RFE—greatly enhanced the stability and accuracy of biomarker identification. As a result, we successfully identified and validated

GPD1 and CEBPD as potential diagnostic and therapeutic targets, offering new insights into the molecular mechanisms of MASLD/MASH and their clinical translation. Furthermore, functional experiments confirmed the key regulatory roles of GPD1 and CEBPD in lipid accumulation and inflammatory responses, underscoring their critical involvement in MASH progression. Mechanistically, GPD1 directly regulates key metabolic and cell cycle pathways, making it a more actionable target for intervention. Furthermore, from the perspective of diagnostic and therapeutic biomarkers, molecules with expression levels above baseline generally provide stronger prognostic and translational value than those below baseline. Therefore, although both genes play important roles, GPD1 has a stronger and more direct impact on disease progression and is upregulated in disease, which is why we prioritized it as a therapeutic target.

Nevertheless, this study has certain limitations. First, the relatively limited sample size in the public databases used may affect the generalizability of the findings. Second, the GEO datasets included in the analysis were primarily derived from Western populations; thus, ethnic and regional differences in gene expression profiles may limit the extrapolation of results to other populations. Future studies involving larger cohorts from Asian, particularly Chinese, populations are needed to strengthen the external validity of our conclusions. It is worth noting, however, that our selection of these publicly available datasets was well-justified: they feature high-quality clinical annotations, sufficient sample sizes, and are widely used in related research, thereby supporting the robustness and reproducibility of our analyses.

In addition, although we preliminarily validated the functional roles of GPD1 and CEBPD through in vivo and in vitro experiments, their precise molecular regulatory mechanisms in MASH remain to be elucidated. Lastly, this study focused primarily on liver tissue and did not explore potential interactions with other key metabolic organs, such as the gut and adipose tissue, which may also play important roles in the systemic pathogenesis of MASLD. Future investigations should incorporate these factors for a more holistic understanding.

Conclusion

This study identified GPD1 and CEBPD as potential biomarkers for MASH, with promising applications in early diagnosis and disease stratification. Their key roles in lipid metabolism and immune regulation underscore their therapeutic potential, suggesting that targeting GPD1 and CEBPD may represent a novel strategy to alleviate inflammation and lipid dysregulation in MASH. By integrating multiple bioinformatics algorithms with comprehensive in vivo and in vitro validation, this study not only highlights the critical involvement of GPD1 in MASH pathogenesis but also elucidates the interplay between lipid metabolic disturbances and immune cell activation, thereby deepening our molecular understanding of MASLD/MASH. These findings provide a theoretical foundation for advancing precision medicine in liver diseases and support the development of non-invasive diagnostic tools and personalized therapeutic strategies. Nonetheless, further mechanistic studies are warranted to elucidate the precise roles of GPD1 and CEBPD and to validate their clinical applicability.

Abbreviation

MASH, Metabolic dysfunction-associated steatohepatitis; DEGs, differentially expressed genes; WGCNA, Weighted gene co-expression network analysis; MASLD, Metabolic dysfunction-associated steatotic liver disease; GPD1, Glycerol-3-phosphate dehydrogenase 1; CEBPD, CCAAT/enhancer-binding protein delta; ROS, reactive oxygen species, GO, Gene Ontology; KEGG, Kyoto Encyclopedia of Genes and Genomes, ssGSEA, Single-Sample Gene Set Enrichment Analysis; siRNA, small interfering RNAs; qPCR, quantitative polymerase chain reaction; WB, Western blotting; IHC, Immunohistochemistry; H&E, hematoxylin and eosin staining; AOD, average optical density.

Data Sharing Statement

These data were derived from the following resources available in the public domain: Gene Expression Omnibus (GEO) database (http://www.ncbi.nlm.nih.gov/geo). The corresponding author can be contacted for further requirements.

Ethics and Dissemination

According to Article 32, Paragraph 1 (research using publicly available data obtained legally, or data generated through observation without interfering with public behavior) and Paragraph 2 (research using anonymized information) of the

Measures for Ethical Review of Life Sciences and Medical Research Involving Human Subjects, issued by China on February 18, 2023, this study is exempt from ethical review. The study utilized publicly available data from the GEO database, and the data sources meet the anonymization requirements. Therefore, this study qualifies for exemption from ethical review and has received exemption approval from the Ethics Committee of Taizhou Central Hospital.

All animal experiments and related procedures were conducted in accordance with internationally recognized guidelines for animal care and were reviewed and approved by the Animal Ethics Committee of Taizhou University. This study strictly complied with local laws, regulations, and institutional requirements.

Funding

This project was supported by the grants from the Medical Science and Technology Project of Zhejiang Province (No. 2025KY444 and No. 2025KY1848) and Taizhou Science and Technology Program for Social Development (23ywa15).

Disclosure

The authors have no conflicts of interest to declare in this work.

References

1. Paik JM, Kabbara K, Eberly KE, Younossi Y, Henry L, Younossi ZM. Global burden of NAFLD and chronic liver disease among adolescents and young adults. *Hepatology*. 2022;75:1204–1217. doi:10.1002/hep.32228
2. De A, Bhagat N, Mehta M, Taneja S, Duseja A. Metabolic dysfunction-associated steatotic liver disease (MASLD) definition is better than MAFLD criteria for lean patients with NAFLD. *J Hepatol*. 2024;80:e61–e62. doi:10.1016/j.jhep.2023.07.031
3. Huang S-C, Liu C-J. Chronic hepatitis B with concurrent metabolic dysfunction-associated fatty liver disease: challenges and perspectives. *Clin Mol Hepatol*. 2023;29:320–331. doi:10.3350/cmh.2022.0422
4. Rinella ME, Lazarus JV, Ratziu V, et al. A multisociety Delphi consensus statement on new fatty liver disease nomenclature. *J Hepatol*. 2023;79:1542–1556. doi:10.1016/j.jhep.2023.06.003
5. Zhang H, Targher G, Byrne CD, et al. A global survey on the use of the international classification of diseases codes for metabolic dysfunction-associated fatty liver disease. *Hepatol Int*. 2024;18:1178–1201. doi:10.1007/s12072-024-10702-5
6. Malekpour M-R, Abbasi-Kangevari M, Ghamari S-H, et al. The burden of metabolic risk factors in North Africa and the Middle East, 1990-2019: findings from the global burden of disease study. *EClinicalMedicine*. 2023;60:102022. doi:10.1016/j.eclinm.2023.102022
7. Owrangi S, Paik JM, Golabi P, et al. Meta-analysis: global prevalence and mortality of cirrhosis in metabolic dysfunction-associated steatotic liver disease. *Aliment Pharmacol Ther*. 2025;61:433–443. doi:10.1111/apt.18451
8. Younossi ZM, Razavi H, Sherman M, et al. Addressing the high and rising global burden of Metabolic Dysfunction-Associated Steatotic Liver Disease (MASLD) and Metabolic Dysfunction-Associated Steatohepatitis (MASH): from the growing prevalence to payors' perspective. *Aliment Pharmacol Ther*. 2025;61:1467–1478. doi:10.1111/apt.70020
9. Hagström H, Shang Y, Hegmar H, Nasr P. Natural history and progression of metabolic dysfunction-associated steatotic liver disease. *Lancet Gastroenterol Hepatol*. 2024;9:944–956. doi:10.1016/S2468-1253(24)00193-6
10. Wang X, Zhang L, Dong B. Molecular mechanisms in MASLD/MASH-related HCC. *Hepatology*. 2024. doi:10.1097/HEP.0000000000000786
11. Nassir F. NAFLD: mechanisms, Treatments, and Biomarkers. *Biomolecules*. 2022;12:824. doi:10.3390/biom12060824
12. Abdelhameed F, Kite C, Lagojda L, et al. Non-invasive scores and serum biomarkers for fatty liver in the era of Metabolic Dysfunction-associated Steatotic Liver Disease (MASLD): a comprehensive review from NAFLD to MAFLD and MASLD. *Curr Obes Rep*. 2024;13:510–531. doi:10.1007/s13679-024-00574-z
13. Hutchison AL, Tavaglione F, Romeo S, Charlton M. Endocrine aspects of metabolic dysfunction-associated steatotic liver disease (MASLD): beyond insulin resistance. *J Hepatol*. 2023;79:1524–1541. doi:10.1016/j.jhep.2023.08.030
14. Feng X, Zhang R, Yang Z, Zhang K, Xing J. Mechanism of metabolic dysfunction-associated steatotic liver disease: important role of lipid metabolism. *J Clin Transl Hepatol*. 2024;12:815–826. doi:10.14218/JCTH.2024.00019
15. Horn P, Tacke F. Metabolic reprogramming in liver fibrosis. *Cell Metab*. 2024;36:1439–1455. doi:10.1016/j.cmet.2024.05.003
16. Bo T, Gao L, Yao Z, et al. Hepatic selective insulin resistance at the intersection of insulin signaling and metabolic dysfunction-associated steatotic liver disease. *Cell Metab*. 2024;36:947–968. doi:10.1016/j.cmet.2024.04.006
17. Liu R, Feng Y, Deng Y, et al. A HIF1α-GPD1 feedforward loop inhibits the progression of renal clear cell carcinoma via mitochondrial function and lipid metabolism. *J Exp Clin Cancer Res*. 2021;40:188. doi:10.1186/s13046-021-01996-6
18. Juszczak GR, Stankiewicz AM. Glucocorticoids, genes and brain function. *Prog Neuropsychopharmacol Biol Psychiatry*. 2018;82:136–168. doi:10.1016/j.pnpbp.2017.11.020
19. Tan Y, Ouyang W, Ma Y, et al. Rare transient infantile hypertriglyceridemia with hypoglycemia and insulin resistance caused by a novel GPD1 mutation. *Mol Syndromol*. 2022;13:433–439. doi:10.1159/000523764
20. Liu P, Cao W, Ma B, et al. Action and clinical significance of CCAAT/enhancer-binding protein delta in hepatocellular carcinoma. *Carcinogenesis*. 2019;40:155–163. doi:10.1093/carcin/bgy130
21. Geng Y, Li Y, Liu G, Jiao J. Identification of biomarkers for the diagnosis in colorectal polyps and metabolic dysfunction-associated steatohepatitis (MASH) by bioinformatics analysis and machine learning. *Sci Rep*. 2024;14:29463. doi:10.1038/s41598-024-81120-8

22. Ma S, Ming Y, Wu J, Cui G. Cellular metabolism regulates the differentiation and function of T-cell subsets. *Cell Mol Immunol*. 2024;21:419–435. doi:10.1038/s41423-024-01148-8
23. Brown EM, Clardy J, Xavier RJ. Gut microbiome lipid metabolism and its impact on host physiology. *Cell Host Microbe*. 2023;31:173–186. doi:10.1016/j.chom.2023.01.009
24. Eslam M, Newsome PN, Sarin SK, et al. A new definition for metabolic dysfunction-associated fatty liver disease: an international expert consensus statement. *J Hepatol*. 2020;73:202–209. doi:10.1016/j.jhep.2020.03.039
25. Deng B, Chen Y, He P, et al. Identification of mitophagy-associated genes for the prediction of metabolic dysfunction-associated steatohepatitis based on interpretable machine learning models. *J Inflamm Res*. 2024;17:2711–2730. doi:10.2147/JIR.S450471
26. Mouskeftara T, Kalopitas G, Liapikos T, et al. A comprehensive analysis of liver lipidomics signature in adults with metabolic dysfunction-associated steatohepatitis-a pilot study. *Int J Mol Sci*. 2024;25:13067. doi:10.3390/ijms252313067
27. Theys C, Ibrahim J, Mateiu L, et al. Mitochondrial GpC and CpG DNA hypermethylation cause metabolic stress-induced mitophagy and cholestophagy. *Int J Mol Sci*. 2023;24:16412. doi:10.3390/ijms242216412
28. Iturbe-Rey S, Maccali C, Arrese M, et al. Lipotoxicity-driven metabolic dysfunction-associated steatotic liver disease (MASLD). *Atherosclerosis*. 2025;400:119053. doi:10.1016/j.atherosclerosis.2024.119053
29. Vassiliou E, Farias-Pereira R. Impact of lipid metabolism on macrophage polarization: implications for inflammation and tumor immunity. *Int J Mol Sci*. 2023;24:12032. doi:10.3390/ijms241512032
30. Peiseler M, Schwabe R, Hampe J, Kubes P, Heikenwälder M, Tacke F. Immune mechanisms linking metabolic injury to inflammation and fibrosis in fatty liver disease - novel insights into cellular communication circuits. *J Hepatol*. 2022;77:1136–1160. doi:10.1016/j.jhep.2022.06.012
31. Aguilar-Ballester M, Herrero-Cervera A, Vinué Á, Martínez-Hervás S, González-Navarro H. Impact of cholesterol metabolism in immune cell function and atherosclerosis. *Nutrients*. 2020;12:2021. doi:10.3390/nu12072021
32. Qiu T, Zhu X, Wu J, Hong W, Hu W, Fang T. Mechanisms of rifaximin inhibition of hepatic fibrosis in mice with metabolic dysfunction associated steatohepatitis through the TLR4/NFκB pathway. *Sci Rep*. 2025;15:9815. doi:10.1038/s41598-025-92282-4
33. Du W, Siwan E, Twigg SM, Min D. Alterations in immune cell profiles in the liver in diabetes mellitus: a systematic review. *Int J Mol Sci*. 2025;26:4027. doi:10.3390/ijms26094027
34. Agarwal H, Wang Y, Tinsley B, Wang X, Ozcan L. RAP1A suppresses hepatic steatosis by regulating amino acid-mediated mTORC1 activation. *JHEP Rep*. 2025;7:101303. doi:10.1016/j.jhepr.2024.101303
35. Cooreman MP, Vonghia L, Francque SM. MASLD/MASH and type 2 diabetes: two sides of the same coin? From single PPAR to pan-PPAR agonists. *Diabetes Res Clin Pract*. 2024;212:111688. doi:10.1016/j.diabres.2024.111688
36. Polchar L, Vallabhaneni P. Case of GPD1 deficiency causing hypertriglyceridaemia and non-alcoholic steatohepatitis. *BMJ Case Rep*. 2022;15:e246369. doi:10.1136/bcr-2021-246369
37. Loomba R, Wong VW-S. Implications of the new nomenclature of steatotic liver disease and definition of metabolic dysfunction-associated steatotic liver disease. *Aliment Pharmacol Ther*. 2024;59:150–156. doi:10.1111/apt.17846
38. Rusu P, Shao C, Neuerburg A, et al. GPD1 specifically marks dormant glioma stem cells with a distinct metabolic profile. *Cell Stem Cell*. 2019;25:241–257.e8. doi:10.1016/j.stem.2019.06.004
39. Basel-Vanagaite L, Zevit N, Har Zahav A, et al. Transient infantile hypertriglyceridemia, fatty liver, and hepatic fibrosis caused by mutated GPD1, encoding glycerol-3-phosphate dehydrogenase 1. *Am J Hum Genet*. 2012;90:49–60. doi:10.1016/j.ajhg.2011.11.028
40. Wang J, Sun X, Jiao L, et al. Clinical characteristics and variant analyses of transient infantile hypertriglyceridemia related to GPD1 gene. *Front Genet*. 2022;13:916672. doi:10.3389/fgene.2022.916672
41. Liu R, Zou Z, Zhang Z, et al. Evaluation of glucocorticoid-related genes reveals GPD1 as a therapeutic target and regulator of sphingosine 1-phosphate metabolism in CRPC. *Cancer Lett*. 2024;605:217286. doi:10.1016/j.canlet.2024.217286